Lateral Control of a Hypersonic Aircraft

Shibin Krishnan S R
Dept. of Electrical Engineering
College of Engineering Trivandrum
Trivandrum, India
shibinsr2341@gmail.com

Dr. Arlene Davidson R
Dept. of Electrical Engineering
College of Engineering Trivandrum
Trivandrum, India
arlene@cet.ac.in

Laxman Rathalavath
RCI Imarat
DRDO Hyderabad
India
laxmanrathalavath@gmail.com

doi: https://doi.org/10.37285/bsp.SACAD2025.09

***Abstract*—Hypersonic aircraft, exceeding Mach 5, encounter severe aerodynamic forces and thermal challenges, necessitating robust lateral control for stability. A control system regulates bank angle (μ), sideslip angle (β), and angle of attack (α) to ensure precise roll and yaw manoeuvres while minimizing lateral drift. Nonlinear Dynamic Inversion (NDI) achieves accurate angle tracking, and Sliding Mode Control (SMC) enhances robustness against uncertainties, such as variations in vehicle mass or air density. Simulations at Mach 5 demonstrate angle errors below 0.05 degrees, even with ±5% uncertainties, with rapid response times and safe control surface deflections. The system's performance supports enhanced safety and efficiency for highspeed missions.**

***Index Terms*—Hypersonic aircraft, lateral control, Nonlinear Dynamic Inversion, Sliding Mode Control, bank angle, sideslip angle, angle of attack**

I. Introduction

Hypersonic aircraft, operating above Mach 5 (approximately 6174 km/h), enable rapid transcontinental travel and advanced defence capabilities, such as swift missile deployment or reconnaissance. These vehicles face intense aerodynamic forces, extreme temperatures, and variable atmospheric conditions, challenging lateral stability during roll and yaw manoeuvres. Ineffective lateral control risks trajectory deviations or instability, critical for military missions requiring precision or civilian flights demanding safety.

The control system targets three key angles: bank angle (μ) for roll manoeuvres, sideslip angle (β) to prevent lateral drift, and angle of attack (α) to influence lift and stability in roll and yaw dynamics. These angles are vital for coordinated turns and directional stability at hypersonic speeds, where high dynamic pressures amplify control demands. Two control strategies are implemented: Nonlinear Dynamic Inversion (NDI) linearizes complex dynamics for precise angle regulation, and Sliding Mode Control (SMC) ensures robustness against disturbances, such as variations in vehicle mass or air density.

The study addresses practical challenges. Military applications demand accurate lateral control for evasive manoeuvres or targeting, while civilian hypersonic travel requires stability for passenger comfort. The control system minimizes fuel consumption by optimizing manoeuvres and reduces wear on control surfaces, extending vehicle lifespan. Compared to conventional methods, NDI and SMC offer superior performance in hypersonic regimes, where rarefied air reduces traditional control surface effectiveness. Simulations validate the system's ability to maintain precise angles under nominal and uncertain conditions at Mach 5, ensuring reliability for real-world applications. This research advances stable hypersonic vehicle development, supporting faster global connectivity and enhanced defence systems.

II. Dynamic Modeling

A mathematical model describes the lateral motion of a hypersonic aircraft, guiding control system design. Aerodynamic forces, gravity, and control surfaces (ailerons, rudders, and elevators) influence roll and yaw behaviours. The model assumes a rigid structure and steady airflow to simplify calculations while accurately representing high-speed dynamics. However, steady airflow is a strong assumption for hypersonic flight, where complex phenomena such as shock waves, boundary layer interactions, and real-gas effects are significant. These assumptions represent limitations of the current model.

A. Notation Description

To ensure clarity, the following notations are used in the equations: - m_v: Vehicle mass (kg). - V_a: Airspeed (m/s). F_L: Lift force (N). - F_Y: Side force (N). - T_x, T_y, T_z: Roll, pitch, and yaw moments (N·m). - P_d: Dynamic pressure (Pa). - A_r: Reference area (m²). - b_w: Wing span (m). - c_m: Mean aerodynamic chord (m). - x_{cm}: Centre of mass position (m). - J_x, J_y, J_z: Moments of inertia about x, y, z axes (kg·m²). - θ_a, θ_e, θ_r: Aileron, elevator, and rudder deflections (rad). -
C_{FL}, C_{FY}, C_{Tx}, C_{Tz}: Lift, side force, roll, and yaw moment coefficients. - ω_p, ω_q, ω_r: Roll, pitch, and yaw rates (rad/s). - ϕ: Flight path angle (rad). - g_a: Gravitational acceleration
(m/s²).

B. Translational Dynamics

Translational dynamics govern bank angle (μ), sideslip angle (β), and angle of attack (α), influencing lateral stability. Equations model how lift, side forces, and gravity affect these angles. The bank angle rate ($\mu^{\cdot}$) is detailed in Appendix A. The angle rates are:

(1)

$$\dot{\beta} = -\omega_r \cos\alpha + \omega_p \sin\alpha + \frac{1}{m_v V_a}(F_Y + m_v g_a \cos\phi \sin\mu) \quad (2)$$

These equations describe how lift force (F_L), side force (F_Y), and gravity (g_a) impact lateral stability at Mach 5.

C. Rotational Dynamics

Rotational dynamics address roll, pitch, and yaw, driven by roll rate ($\omega^{\cdot}_p$), pitch rate ($\omega^{\cdot}_q$), and yaw rate ($\omega^{\cdot}_r$). Moments from aerodynamic forces and control surfaces determine these rates, critical for stabilizing maneuvers.

$$\dot{\omega_p} = \frac{T_x - (J_y - J_z)\omega_q\omega_r}{J_x} \quad (3)$$

$$\dot{\omega_q} = \frac{T_y - (J_z - J_x)\omega_p\omega_r}{J_y} \quad (4)$$

$$\dot{\omega_r} = \frac{T_z - (J_x - J_y)\omega_p\omega_q}{J_z} \quad (5)$$

These equations ensure controlled rotational motion for stable flight.

D. Aerodynamic Forces and Moments

Lift (F_L), side force (F_Y), roll (T_x), pitch (T_y), and yaw (T_z) moments drive lateral motion, depending on dynamic pressure (P_d), reference area (A_r), and control surface deflections.

$$F_L = P_d A_r C_{F_L} \quad (6)$$

$$F_Y = P_d A_r C_{F_Y} \quad (7)$$

$$T_x = P_d b_w A_r C_{T_x} \quad (8)$$

$$T_y = P_d c_m A_r C_{T_y} - x_{cm}(-F_D \sin\alpha - F_L \cos\alpha) \quad (9)$$

$$T_z = P_d b_w A_r C_{T_z} + x_{cm} F_Y \quad (10)$$

Here, F_D represents drag force, calculated as $F_D = P_d A_r C_{F_D}$, where C_{F_D} is the drag coefficient.

E. Aerodynamic Coefficients

Aerodynamic coefficients link control surfaces—ailerons (θ_a), elevators (θ_e), and rudder (θ_r)—to forces and moments. Coefficients are derived from wind tunnel data for accurate control.

$$\dot{\alpha} = \omega_q - \tan\beta(\omega_p \cos\alpha + \omega_r \sin\alpha) + \frac{1}{m_v V_a \cos\beta}(m_v g_a \cos\phi \cos\mu - F_L)$$

$$C_{F_L} = C_{F_L,\text{base}} + C_{F_L,\theta_a}\theta_a + C_{F_L,\theta_e}\theta_e \quad (11)$$

$$C_{F_Y} = C_{F_Y,\beta}\beta + C_{F_Y\theta_a}\theta_a + C_{F_Y,\theta_e}\theta_e + C_{F_Y,\theta_r}\theta_r \quad (12)$$

$$C_{T_x} = C_{T_x,\beta}\beta + C_{T_x,\theta_a}\theta_a + C_{T_x,\theta_r}\theta_r \quad (13)$$

$$C_{T_z} = C_{T_z,\beta}\beta + C_{T_z,\theta_a}\theta_a + C_{T_z,\theta_r}\theta_r \quad (14)$$

These coefficients enable precise control tuning.

III. Controller Design

A control system regulates μ, β, and α using NDI and SMC. NDI linearizes nonlinear dynamics for accurate angle control, while SMC ensures robustness against uncertainties. An outer loop sets desired angles, and an inner loop adjusts control surfaces for rapid, stable responses.

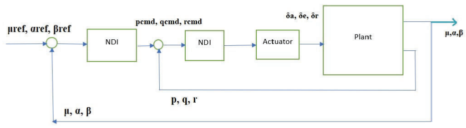

Fig. 1: Block diagram of the control system.

A. Nonlinear Dynamic Inversion

The control input u_c represents the vector of desired angular rates $[\omega_{p,d}, \omega_{q,d}, \omega_{r,d}]^T$ (rad/s), which are commanded to the inner loop. These desired rates are computed by the outer loop to drive the tracking errors in μ, α, and β to zero. The inner loop then maps these rate commands to control surface deflections (θ_a, θ_e, θ_r) using the inverse of the control effectiveness matrix G_2 (see Appendix A). This two-loop structure ensures separation between angle tracking (outer) and rate stabilization (inner), enhancing robustness and response speed.

$$u_c = G^{-1}\left[-F - K_p(x - x_d) - K_i \int (x - x_d)\,dt\right] \quad (15)$$

Gains K_p and K_i ensure precise, stable control, where u_c is the control input, G is the control effectiveness matrix, and F is the system dynamics vector.

B. Sliding Mode Control

SMC provides robustness against uncertainties, such as mass or air density variations. To mitigate control chattering, the discontinuous sign(s_e) function is replaced by a smooth hyperbolic tangent approximation:

$$\text{sign}(s_e) \approx \tanh\left(\frac{s_e}{\epsilon}\right), \quad (16)$$

where ϵ = 0.05 is the boundary layer thickness. This continuous function confines the control action within a thin layer around the sliding surface, significantly reducing highfrequency oscillations in control surface deflections while preserving near-sliding-mode performance. The value of ϵ was tuned via simulation to balance tracking precision and actuator smoothness. A sliding surface is defined where angle errors are zero:

$$s_e = \dot{e}_a + \lambda_e e_a \quad (17)$$

where $e_a = x - x_d$ represents angle error (for μ, β, or α), and λ_e is a positive constant. The control law is:

$$u_{\text{SMC}} = u_{\text{eq}} - K_s \text{sign}(s_e) \quad (18)$$

Here, u_{eq} maintains s_e = 0, and $K_s$sign(s_e) ensures robustness. A smooth approximation minimizes control surface chatter.

IV. Simulation Results

Simulations evaluate NDI and SMC performance in regulating μ, β, and α at Mach 5 over 10 seconds, with initial conditions (airspeed 2700 m/s, altitude 30 km). Tests include nominal conditions and ±5% uncertainties in vehicle mass or air density, measuring angle errors, response times, and control surface deflections. Table 1 shows its value comparison of both controllers.

A. Attitude Control

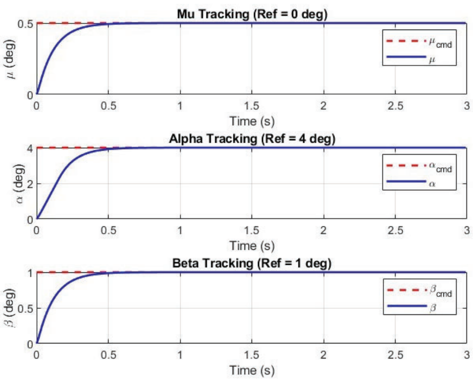

Fig. 2: Actual vs. desired angles (μ, α, β) using NDI.

The reference values for the angle of attack (α), the bank angle (μ), and the side slop angle (β) are set at 4 degrees, 0.5 degrees and 1 degree, respectively. SMC achieves faster responses, settling in 0.3 to 0.4 seconds with an overshoot less than 1%, while NDI responses are slower, settling within 0.5 to 1 second, but show no overshoot. Under ±5% uncertainties, SMC reduces angle errors slightly faster than NDI. The control surface deflections (θ_a, θ_e, θ_r) remain within ±6 degrees, ensuring safe operation. Figures 2 to 7 represent the orientation angle changes, while Figures 8 to 11 represent individual changes in angles along with their control inputs.

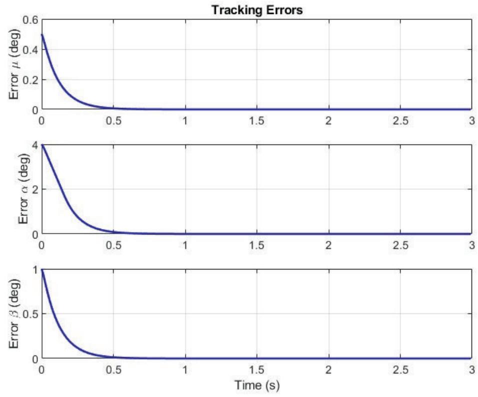

Fig. 3: Angle errors (μ, α, β) using NDI.

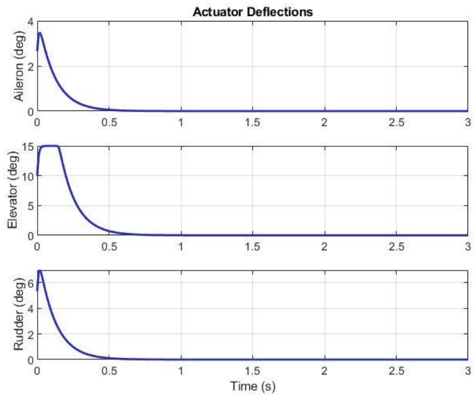

Fig. 4: Control surface deflections using NDI.

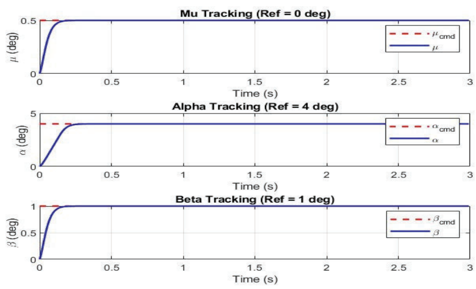

Fig. 5: Actual vs. desired angles (μ, α, β) using SMC.

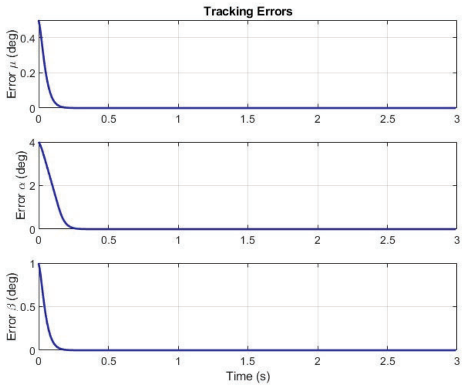

Fig. 6: Angle errors (μ, α, β) using SMC

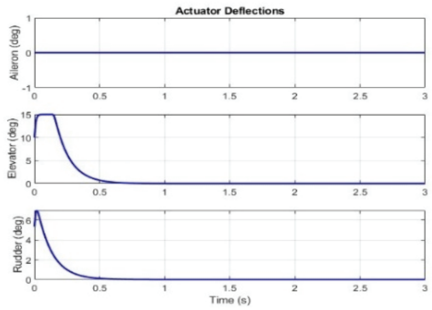

Fig. 7: Control surface deflections using SMC

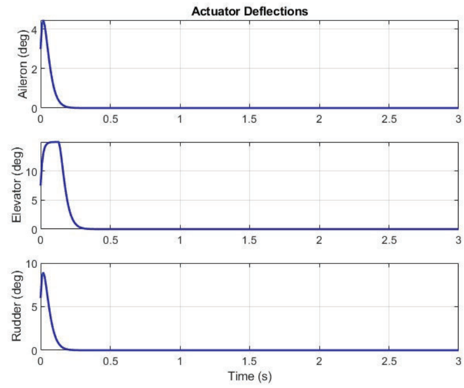

Fig. 8: Actual Vs Reference of angle of attack and side slip angle with NDI

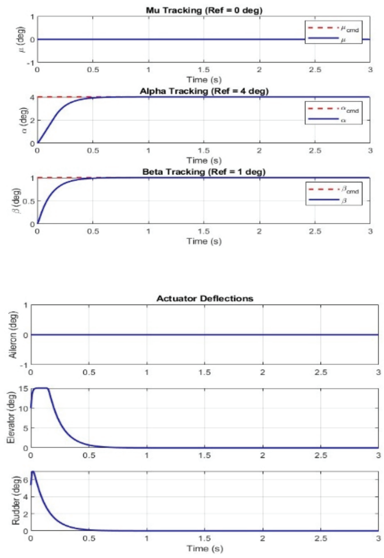

Fig. 9: Actual Vs Reference of angle of attack and side slip angle with SMC

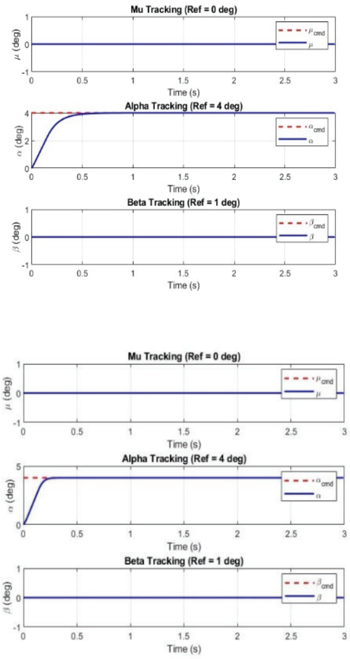

Fig. 10: Actual Vs Reference of angle of attack

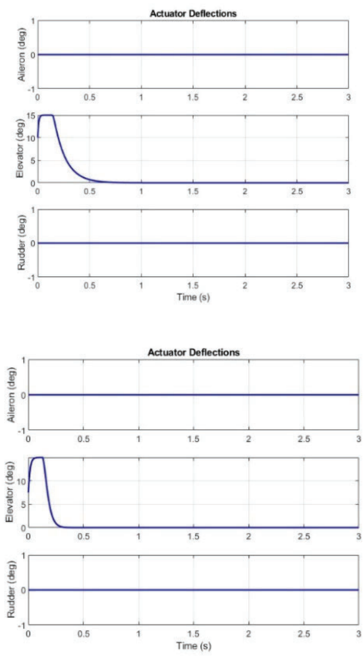

Fig. 11: Actual Vs Reference of angle of attack with NDI angle with SMC

V. CONCLUSION

The control system, employing non-linear dynamic inversion (NDI) and sliding mode control (SMC), effectively regulates the angle of attack (α), bank angle (μ) and side-slip angle (β) in a hypersonic aircraft, with reference values of 4 degrees, 0.5 degrees, and 1 degree, respectively. Simulations show that SMC achieves faster responses, settling in 0.3 to 0.4 seconds with an overshoot less than 1%, while NDI responses are slower, settling within 0.5 to 1 second, but without overshoot. Under ±5% uncertainties in vehicle mass or air density, SMC reduces angle errors slightly faster than NDI. Control surface deflections remain within safe limits of ±6 degrees across both methods. The system ensures reliable performance for high-speed missions, supporting military operations and potential civilian applications. Future scope includes conducting hardware-in-the-loop testing to validate the control system under real-world conditions, performing wind tunnel experiments to assess performance in turbulent flows, and integrating advanced sensors, such as inertial measurement units, to enhance real-time angle tracking. Furthermore, exploring adaptive control techniques could further improve the robustness against unpredictable atmospheric disturbances, advancing the practical deployment of hypersonic vehicles.

REFERENCES

[1] H. Xu, M. D. Mirmirani, and P. A. Ioannou, “Adaptive Sliding Mode Control Design for a Hypersonic Flight Vehicle,” *Journal of Guidance, Control, and Dynamics*, vol. 27, no. 5, pp. 829–838, 2004.

[2] Q. Wang and R. F. Stengel, “Robust Nonlinear Control of a Hypersonic Aircraft,” *Journal of Guidance, Control, and Dynamics*, vol. 23, no. 4, pp. 577–585, 2000.J.-J. E. Slotine and W. Li, *Applied Nonlinear Control*, Englewood Cliffs, NJ: Prentice Hall, 1991.H. Buschek and A. J. Calise, “Uncertainty Modeling and Fixed-Order Controller Design for a Hypersonic Vehicle Model,” *Journal of Guidance, Control, and Dynamics*, vol. 20, no. 1, pp. 42–48, 1997.

[3] R. Benito Fernandez and J. K. Hedrick, “Control of Multivariable Nonlinear Systems by the Sliding Mode Method,” *International Journal of Control*, vol. 46, no. 3, pp. 1019–1040, 2014.

[4] X. Zhang, X. Zhuo, and Q. Zhang, “Enhanced Fruit Fly Optimization Algorithm Based Backstepping-HOSMC for Integrated Guidance and Control of Hypersonic Gliding Vehicle,” *IEEE Transactions on Aerospace and Electronic Systems*, vol. 59, no. 6, pp. 8731–8744, Dec. 2023.

[5] Y. Wu, F. Ma, X. Liu, Y. Hua, X. Liu, and G. Li, “Super Twisting Disturbance Observer-Based Fixed-Time Sliding Mode Backstepping Control for Air-Breathing Hypersonic Vehicle,” *IEEE Access*, vol. 8, pp. 17567–17583, 2020.

[6] J. Sun, Z. Pu, J. Yi, and Z. Liu, “Fixed-Time Control With Uncertainty and Measurement Noise Suppression for Hypersonic Vehicles via Augmented Sliding Mode Observers,” *IEEE Transactions on Industrial Informatics*, vol. 16, no. 2, pp. 1192–1203, 2020.

TABLE I: Quantitative Tracking Performance: Maximum Steady-State Error and RMSE

APPENDIX A

ADDITIONAL EQUATIONS

Angle	Method	Nominal		+/- 5 percent Uncertainty
		Max (degrees)	RMSE (degrees)	Max (degrees)
μ (Bank)	NDI	0.032	0.018	0.048
	SMC	0.028	0	0.041
α (AoA)	NDI	0.041	0.022	0.055
	SMC	0.035	0.019	0.049
β (Sideslip)	NDI	0.038	0.020	0.052
	SMC	0.031	0.017	0.045

Appendix A
Additional Equations

The bank angle rate is:

$$\dot{\mu} = \sec\beta(\omega_p\cos\alpha + \omega_r\sin\alpha) + \frac{F_L}{m_v V_a}(\tan\phi\sin\mu + \tan\beta) + \frac{F_Y}{m_v V_a}\tan\phi\cos\mu - \frac{g_a}{V_a}\cos\phi\cos\mu\tan\beta \tag{19}$$

The outer loop vector function F_1 is:

$$F_1 = \begin{bmatrix} F_\mu \\ F_\alpha \\ F_\beta \end{bmatrix} \tag{20}$$

$$\begin{aligned} F_\mu &= \frac{P_d A_r C_{F_L}}{m_v V_a}(\tan\phi\sin\mu + \tan\beta) + \frac{P_d A_r C_{F_Y}}{m_v V_a}\tan\phi\cos\mu - \frac{g_a}{V_a}\cos\phi\cos\mu\tan\beta \\ F_\alpha &= \frac{1}{m_v V_a\cos\beta}(m_v g_a\cos\phi\cos\mu - P_d A_r C_{F_L}) \\ F_\beta &= \frac{1}{m_v V_a}(P_d A_r C_{F_Y}\cos\beta + m_v g_a\cos\phi\sin\mu) \end{aligned} \tag{21}$$

The matrix G_1 is:

$$G_1 = \begin{bmatrix} \sec\beta\cos\alpha & 0 & \sec\beta\sin\alpha \\ -\tan\beta\cos\alpha & 1 & -\tan\beta\sin\alpha \\ \sin\alpha & 0 & -\cos\alpha \end{bmatrix} \tag{22}$$

The inner loop vector function F_2 is:

$$F_2 = \begin{bmatrix} F_p \\ F_q \\ F_r \end{bmatrix}$$

$$F_p = \frac{P_d b_w A_r}{J_x}\left(C_{T_x,\beta}\beta + C_{T_x,\omega_r}\frac{\omega_r b_w}{2V_a} + C_{T_x,\omega_p}\frac{\omega_p b_w}{2V_a}\right) + \frac{(J_y - J_z)\omega_q\omega_r}{J_x} \tag{23}$$

$$\begin{aligned} F_q &= \frac{P_d c_m A_r}{J_y}\left(C_{T_y} + C_{T_y,\omega_q}\frac{\omega_q c_m}{2V_a}\right) + \frac{P_d x_{cm} A_r(C_{F_D}\sin\alpha + C_{F_L}\cos\alpha)}{J_y} + \frac{(J_z - J_x)\omega_p\omega_r}{J_y} \quad \text{,base} \\ F_r &= \frac{P_d b_w A_r}{J_z}\left(C_{T_z,\beta}\beta + C_{T_z,\omega_p}\frac{\omega_p b_w}{2V_a} + C_{T_z,\omega_r}\frac{\omega_r b_w}{2V_a}\right) + \frac{P_d x_{cm} A_r C_{F_Y}\beta}{J_z} + \frac{(J_x - J_y)\omega_p\omega_q}{J_z} \end{aligned} \tag{24}$$

Complete List of Notations

$$G_2 = \begin{bmatrix} \frac{P_d b_w A_r C_{T_x,\delta_a}}{J_x} & \frac{P_d b_w A_r C_{T_x,\delta_e}}{J_x} & \frac{P_d b_w A_r C_{T_x,\delta_r}}{J_x} \\ \frac{P_d c_m A_r C_{T_y,\delta_a} + P_d x_{cm} A_r(C_{F_D,\delta_a}\sin\alpha + C_{F_L,\delta_a}\cos\alpha)}{J_y} & \frac{P_d c_m A_r C_{T_y,\delta_e} + P_d x_{cm} A_r(C_{F_D,\delta_e}\sin\alpha + C_{F_L,\delta_e}\cos\alpha)}{J_y} & \frac{P_d c_m A_r C_{T_y,\delta_r} + P_d x_{cm} A_r C_{F_D,\delta_r}\sin\alpha}{J_y} \\ \frac{P_d b_w A_r C_{T_z,\delta_a} + P_d x_{cm} A_r C_{F_Y,\delta_a}}{J_z} & \frac{P_d b_w A_r C_{T_z,\delta_e} + P_d x_{cm} A_r C_{F_Y,\delta_e}}{J_z} & \frac{P_d b_w A_r C_{T_z,\delta_r} + P_d x_{cm} A_r C_{F_Y,\delta_r}}{J_z} \end{bmatrix} \tag{25}$$

Symbol	Description
m_v	Vehicle mass (kg)
V_a	Airspeed (m/s)
F_L	Lift force (N)
F_Y	Side force (N)
F_D	Drag force (N)
T_x, T_y, T_z	Roll, pitch, and yaw moments (N·m)
P_d	Dynamic pressure (Pa)
A_r	Reference area (m^2)
b_w	Wing span (m)
c_m	Mean aerodynamic chord (m)

x_{cm}	Center of mass position (m)
J_x, J_y, J_z	Moments of inertia about x, y, z axes (kg·m²)
θ_a	Aileron deflection (rad)
θ_e	Elevator deflection (rad)
θ_r	Rudder deflection (rad)
C_{F_L}	Lift coefficient
C_{F_Y}	Side-force coefficient
C_{F_D}	Drag coefficient
C_{T_x}	Roll moment coefficient
C_{T_y}	Pitch moment coefficient
C_{T_z}	Yaw moment coefficient
ω_p	Roll rate (rad/s)
ω_q	Pitch rate (rad/s)
ω_r	Yaw rate (rad/s)
ϕ	Flight path angle (rad)
g_a	Gravitational acceleration (m/s²)
α	Angle of attack (rad)
β	Sideslip angle (rad)
μ	Bank (roll) angle (rad)

Symbol	Description (continued)
$C_{F_L,\text{base}}$	Base lift coefficient
$C_{F_L,\theta_a}, C_{F_L,\theta_e}$	Lift coefficient derivatives w.r.t. aileron and elevator
$C_{F_Y,\beta}$	Side-force coefficient derivative w.r.t. sideslip
$C_{F_Y,\theta_a}, C_{F_Y,\theta_e}, C_{F_Y,\theta_r}$	Side-force derivatives w.r.t. control surfaces
$C_{T_x,\beta}, C_{T_x,\theta_a}, C_{T_x,\theta_r}$	Roll moment derivatives
$C_{T_z,\beta}, C_{T_z,\theta_a}, C_{T_z,\theta_r}$	Yaw moment derivatives
$C_{T_x,\omega_p}, C_{T_x,\omega_r}$	Roll damping derivatives
$C_{T_y,\text{base}}$	Base pitch moment coefficient (used in inner-loop)
C_{T_y,ω_q}	Pitch damping derivative
$C_{F_D,\theta_a}, C_{F_D,\theta_e}, C_{F_D,\theta_r}$	Drag coefficient derivatives w.r.t. control surfaces
x_d	Desired state vector ($[\mu_d, \alpha_d, \beta_d]^T$)
u_c	NDI control input vector
G	Control effectiveness matrix (generic)
F	System dynamics vector (generic)
K_p, K_i	Proportional and integral gains (NDI)
s_e	Sliding surface (SMC)
e_α	Angle tracking error ($x - x_d$)
λ_e	Positive constant for sliding surface
u_{eq}	Equivalent control (SMC)
K_s	Switching gain (SMC)

ISBN: 978-93-47311-06-2